scientific reports

Check for updates

OPEN

A comparative study on the efficacy of two different types of intracranial stent retrievers based on finite element simulation

Yong Wu[1], Kejia Zhao[2], Yunhan Cai[3], Yibin Fang[4]✉ & Shengzhang Wang[1,2,3]✉

This study investigates the thrombectomy performance of open (Solitaire FR 6 × 30) and closed (Trevo XP ProVue 6 × 25) stent retrievers in patient-specific vasculature using finite element analysis (FEA). The aim is to inform stent design optimization and improve surgical strategies. Patient-specific vascular models, thrombus models, and stent retriever models were constructed using CAD software. FEA simulated the thrombectomy procedure, and the simulation results were validated through in vitro experiments. The FEA predicted successful thrombus retrieval with the Solitaire FR 6 × 30, consistent with in vitro findings. Conversely, the Trevo XP ProVue 6 × 25 failed to retrieve the thrombus in the simulation. During Solitaire FR 6 × 30 thrombectomy, maximum thrombus stress (48.733 MPa), strain (2.257) and contact pressure on the vessel wall (7.177 MPa) were substantially higher than those observed during Trevo XP ProVue 6 × 25 thrombectomy (15.824 MPa, 1.554, and 1.872 MPa, respectively). Specifically, the Solitaire FR 6 × 30 induced 3.19 times greater maximum thrombus stress, 1.45 times greater maximum thrombus strain, and 2.83 times greater maximum vessel wall contact pressure. These findings suggest that the Solitaire FR stent retriever demonstrates superior thrombectomy efficacy compared to the Trevo XP stent retriever, likely attributable to its higher radial support force. However, the increased force exerted on the thrombus and vessel wall by the Solitaire FR raises the potential risk of thrombus fragmentation and vascular injury.

Keywords Ischemic stroke, Stent retriever, Finite element simulation, In vitro experiment

Acute ischemic stroke, typically resulting from thromboembolic occlusion of cerebral arteries (e.g., by plaque composed of fatty substances including cholesterol), necessitates rapid restoration of blood flow. Two primary treatment strategies exist: thrombolytic drug therapy and mechanical thrombectomy (MT). Thrombolytic agents are effective within a limited 3–6 h window post-stroke onset, and certain thrombi prove resistant to pharmacological dissolution[1]. Advancements in cerebrovascular intervention have led to the widespread adoption of MT, which extends the therapeutic window to 6–24 h and offers advantages in terms of higher reperfusion rates and shorter reperfusion times[2]. Stent retrievers are the most common devices employed in MT and represent the highest level of recommendation for specific patient populations in both national and international guidelines[3].

The thrombectomy procedure involves crimping a stent retriever within a microcatheter for delivery. Upon reaching the target thrombus, the stent is deployed by retracting the microcatheter, allowing the stent to expand and ensnare the thrombus, which is subsequently retrieved using a receiving catheter. This intricate mechanical process carries the potential for complications. Excessive stress and strain during crimping within the microcatheter can lead to inaccurate deployment or even stent fracture[4]. Post-expansion, high stresses on the vessel wall may induce vascular damage, spasm, or rupture leading to hemorrhage[5,6]. Furthermore, insufficient stent-thrombus contact during retrieval can result in thrombus fragmentation and distal embolization[4]. Consequently, numerous studies have investigated stent retriever performance and the complex interaction between stent, thrombus, and vessel wall using both in vitro experiments and computational simulations[7,8].

In vitro studies have focused extensively on optimizing thrombectomy techniques and stent retriever design. A key finding is the importance of aligning the proximal ends of the stent retriever and the thrombus

[1]Yiwu Research Institute of Fudan University, Zhejiang, China. [2]Institute of Biomedical Engineering Technology, School of Engineering and Applied Technology, Fudan University, Shanghai, China. [3]Institute of Biomechanics, Department of Aeronautics and Astronautics, Fudan University, Shanghai, China. [4]Tongji University Affiliated Shanghai Fourth People's Hospital, Shanghai, China. ✉email: fangyibin@163.com; szwang@fudan.edu.cn

for maximizing device-thrombus contact during deployment, thereby enhancing retrieval efficacy[9]. Adequate radial support is essential for effective thrombus traction during the procedure[10,11]. Moreover, open design stent retrievers appear advantageous for retrieving high-friction, fibrin-rich thrombi, as they facilitate more complete device-thrombus contact and improve thrombectomy success rates[12].

Computational simulations employing various numerical methods, including finite element analysis (FEA), computational fluid dynamics (CFD), fluid-structure interaction (FSI), and lumped parameter models, have been used to investigate the complex interaction between stent retrievers, thrombi, and blood vessels, as well as the influence of blood flow on the thrombus. Studies using idealized deformable vessel and thrombus models have explored stent retriever performance under realistic retraction forces and assessed device-vessel wall adhesion during retrieval[13]. FEA has been employed to analyze the biomechanical properties of both closed and open stent retriever designs[14,15], and to propose device optimization strategies[16]. Patient-specific vascular models have also been utilized to simulate mechanical thrombectomy procedures[7]. Accurate representation of thrombus mechanical behavior is critically dependent on the chosen constitutive model. While the Mooney-Rivlin hyperelastic model is frequently employed, it can deviate significantly from observed thrombus behavior under large deformations. Alternative approaches include biphasic models representing fibrin and cells as solid and fluid phases, respectively, to study thrombus rupture[17], and viscoelastic, incompressible models using FEA Lagrangian methods[18]. Luraghi employed a simplified compressible hyperelastic foam model based on a uniaxial load curve from Fereidoonnezhad's unconfined compression test, demonstrating accurate reproduction of thrombus mechanical behavior under large deformation[19].

This study establishes a novel model for simulating stent retriever thrombectomy. Using this model, a comparative analysis of open and closed stent retriever performance in patient-specific vasculature was conducted, and the interactions between the stent retriever, thrombus, and vessel wall were quantitatively evaluated.

Results

Comparison between in vitro experimental results and finite element simulation results

Both experimental and simulation results (Fig. 1) show that Solitaire FR 6 × 30 removes the thrombus successfully. The thrombus is dragged and moved towards the proximal end of the blood vessels. The deformation of the thrombus in the simulation is informative. Although tortuosity of the blood vessels increases the complexity of simulation, the results are still consistent with the experimental results.

After verifying finite element simulation of the thrombectomy procedure through in vitro experiments, a similar method was used to simulate the thrombectomy procedure of Trevo XP and a comparison was made between Solitaire FR and Trevo XP, as shown in Fig. 2. In the simulation of Solitaire FR 6 × 30, the thrombus moves with the stent to the proximal end of the blood vessels and successfully passes through C4 segment of the internal carotid artery. In the simulation of Trevo XP ProVue 6 × 25, at the end of the thrombectomy procedure, the thrombus detaches from the stent and doesn't pass through the C4 segment, resulting in thrombectomy failure. The simulation results show that Solitaire FR 6 × 30 with an open design can better adapt to tortuous blood vessels and remove thrombus successfully. While Trevo XP ProVue 6 × 25 is also used for thrombectomy clinically, it may need more delicate operation, which wasn't realized in our simulation.

Stress and strain on thrombus

Figure 3 shows the maximum first principal stress and maximum first principal strain on the thrombus during the thrombectomy procedure. During the Solitaire FR 6 × 30 thrombectomy, maximum stress (48.733 MPa) and

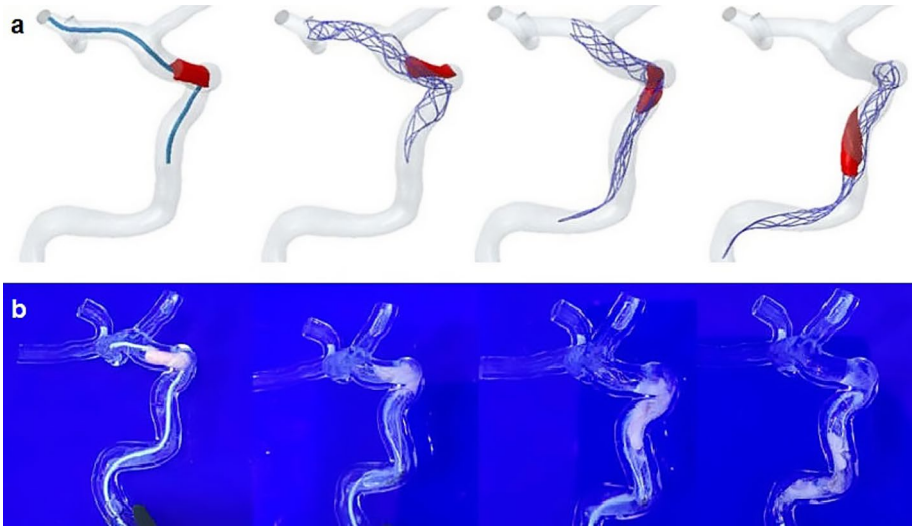

Fig. 1. Comparison between simulation and experimental results of Solitaire FR 6 × 30 thrombectomy. a, Simulation results; b, Experimental results.

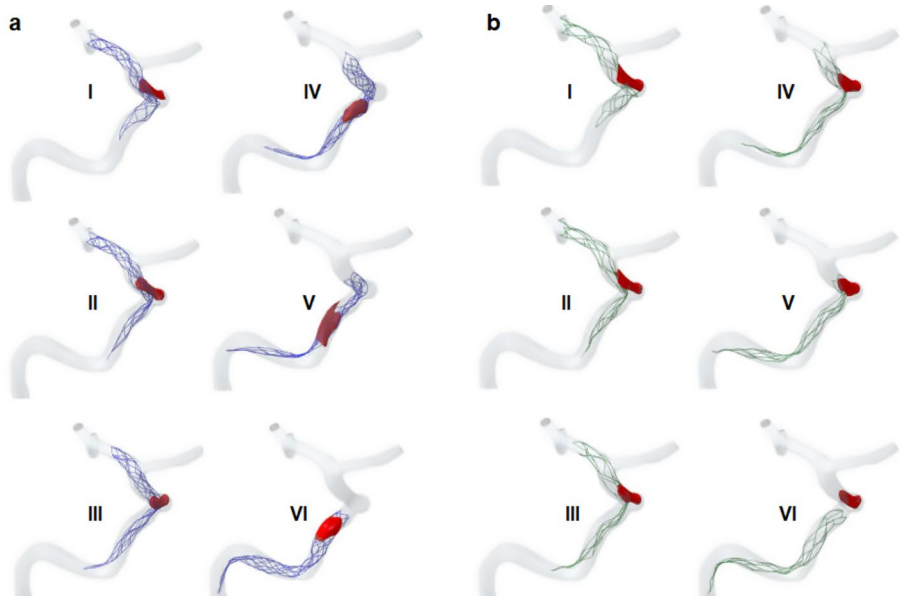

Fig. 2. Deformation of thrombus during thrombectomy procedure. a, Solitaire FR 6 × 30; b, Trevo XP ProVue 6 × 25. I, At the beginning of the thrombectomy procedure; II, III, IV, V, During the thrombectomy procedure; VI, At the end of the thrombectomy procedure.

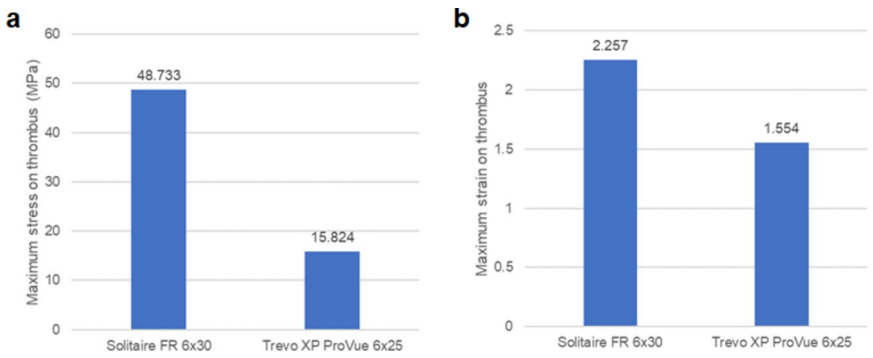

Fig. 3. Maximum stress and strain on thrombus during thrombectomy procedure with different stents. a, Maximum stress; b, Maximum strain.

strain (2.257) on the thrombus are 3.19 and 1.45 times higher than those during the Trevo XP ProVue 6 × 25 thrombectomy, which are 15.824 MPa and 1.554 respectively. This indicates that the thrombus has a stronger interaction with Solitaire FR 6 × 30, that's to say, the thrombus has greater chance to move with the stent against other resistance, such as blood flow rush and blood vessel wall shear force, which may be the reason why Solitaire FR 6 × 30 can successfully remove the thrombus, as well as a greater risk of breaking the thrombus.

Contact pressure on the vascular wall

During the Solitaire FR 6 × 30 thrombectomy procedure, the maximum contact pressure (7.177 MPa) on the vascular wall is 2.83 times higher than that during the Trevo XP ProVue 6 × 25 thrombectomy procedure, which is 1.872 MPa. This indicates that Solitaire FR 6 × 30 has a stronger interaction with the blood vessels, and of course, the risk of vascular damage is also higher.

Discussion

The Solitaire, an open stent retriever with an overlapping cross-sectional design, facilitates thrombus engagement on multiple planes, enhancing fixation[20]. Its variable radial support force maximizes vessel revascularization upon initial deployment and minimizes intimal damage after full deployment. The overlapping structure also contributes to improved stent adhesion, flexibility, and compliance, enabling adaptation to tortuous vessels and those with varying diameters[20]. However, significant distal end deformation[21]poses a risk of distal vessel injury and embolism[22], despite its frequent use as a first-line thrombectomy device in large vessels[23].

The Trevo, a closed non-overlapping spiral mesh stent retriever, offers greater radial support and stronger capture of hard thrombi[20], potentially extending the treatment window. Its conical head and tail transitions, combined with reduced metal coverage, result in a softer profile compared to the Solitaire[21]. Full device visualization during deployment facilitates precise control, minimizing excessive pulling and bleeding risks[24]. Its design is well-suited for thrombectomy in finer distal vessels[22,25].

This study simulated Solitaire FR 6×30 and Trevo XP ProVue 6×25 thrombectomy procedures within patient-specific vessel models, validating the simulations with in vitro experiments (for the Solitaire device). Results indicated substantially higher maximum thrombus stress (48.733 MPa vs. 15.824 MPa), thrombus strain (2.257 vs. 1.554), and vessel wall contact pressure (7.177 MPa vs. 1.872 MPa) during Solitaire thrombectomy compared to Trevo. The successful Solitaire thrombectomy correlated with greater device expansion and stronger thrombus-vessel interaction, while the unsuccessful Trevo deployment exhibited incomplete expansion and a persistent gap between the device and vessel wall, suggesting weaker thrombus capture. These findings underscore the importance of robust device-thrombus-vessel interaction for successful thrombectomy. However, further research is needed to optimize thrombus removal while mitigating risks of rupture and vessel damage.

This study's limitations include: (a) simplifications in the model, such as assuming rigid vessel walls; (b) neglecting the influence of blood flow; and (c) the lack of in vitro validation for the Trevo simulations. Future research will address these limitations.

Conclusions

This study compared the performance of open and closed stent retrievers (Solitaire FR 6×30 and Trevo XP ProVue 6×25, respectively) in patient-specific vasculature using computational simulations validated by in vitro experiments (for the Solitaire device). Simulations predicted successful thrombus retrieval with the Solitaire, consistent with in vitro observations, while the Trevo failed to retrieve the thrombus. Quantitative analysis revealed significantly higher maximum thrombus stress (48.733 MPa vs. 15.824 MPa), thrombus strain (2.257 vs. 1.554), and vessel wall contact pressure (7.177 MPa vs. 1.872 MPa) during Solitaire thrombectomy compared to Trevo.

Materials and methods

Modeling of intracranial stent retrievers

This paper established two types of stent retriever models (Table 1), including an open stent Solitaire FR 6×30 and a closed stent Trevo XP ProVue 6×25.

The specific modeling method for Solitaire FR 6×30 is as follows:

1. Unfold the stent and measure the overall size and repetitive unit size.
2. Establish a 2D planar geometric model of the stent in the CAD software SolidWorks 2018 (Dassault System, France), and then import the model into ABAQUS/CAE 2018 (Dassault System, France) for geometric cleaning.
3. Based on the sensitivity analysis of grid size, use B31 elements with an average length of 0.2 mm to mesh the model.
4. Curl the 2D planar mesh model into a cylindrical 3D mesh model.

The process of establishing the Trevo XP ProVue 6×25 model is roughly the same as that of Solitaire FR 6×30. While the Trevo XP ProVue 6×25 is a closed stent, it needs to be cut before measurement. After being curled into a 3D mesh model, those cut nodes need to be combined with mesh editing tools.

Two types of stent models are shown in Fig. 4.

Then, a microcatheter model was established with an inner diameter of 0.7 mm and S4R shell elements were used to mesh.

Hyperelastic nickel titanium alloy material integrated in ABAQUS/CAE 2018 was selected for the stents, and the initial parameters of the material were taken from previous studies[26]. Afterwards, radial support force of the stents was tested using the Blockwise Crimping System (Blockwise Engineering, USA), and material parameters were calibrated based on experimental data. Final material parameters used are shown in Table 2.

Modeling of patient-specific blood vessels

The patient-specific cerebrovascular model is based on CT angiography data, which was ethically approved by Central Hospital of Jingan District, Shanghai. Specific modeling steps are as follows:

1. Import the patient's CTA image data into Mimics Medical 21.0 (Materialise, Belgium). Segment the vascular area and export.
2. Import the vascular area into Geomagic Wrap 2015 (Raindrop, USA). Capture the segment between right internal carotid artery and middle cerebral artery M2. Smooth the captured blood vessels to ensure no intersecting patches or punctures.

Type	Diameter (mm)	Effective length (mm)	Total length (mm)
Solitaire FR 6×30	6	30	42
Trevo XP ProVue 6×25	6	25	40

Table 1. Parameters of stent retrievers.

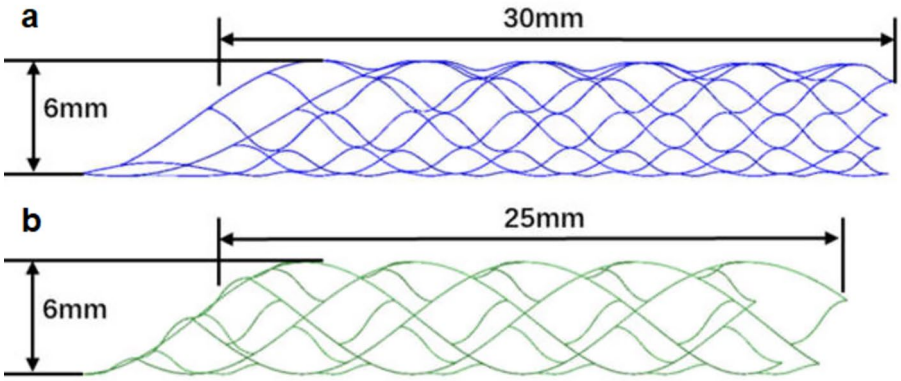

Fig. 4. Models of different stent retrievers. a, Solitaire FR 6×30; b, Trevo XP ProVue 6×25.

Symbol	Parameter	Solitaire FR 6×30	Trevo XP ProVue 6×25
E_A	Austenite Young's modulus	60,000 MPa	56,000 MPa
ϑ_A	Austenite Poisson's Ratio	0.3	0.3
E_M	Martensite Young's modulus	47,800 MPa	23,700 MPa
ϑ_M	Martensite Poisson's Ratio	0.3	0.3
ϵ^L	Transformation strain	0.063	0.063
σ_L^S	Loading start of transformation stress	600 MPa	635 MPa
σ_L^E	Loading end of transformation stress	670 MPa	677 MPa
σ_U^S	Unloading start of transformation stress	288 MPa	288 MPa
σ_U^E	Unloading end of transformation stress	254 MPa	254 Mpa
T	Temperature	37℃	37℃

Table 2. Parameters of nickel titanium alloy material.

3. Measure the inner diameter of the smoothed blood vessels and export.
4. Import the smoothed blood vessels into HyperMesh 2021 to mesh, and then import it into ABAQUS/CAE 2018 (Fig. 5).

The patient-specific vascular model is assumed to be rigid. In vitro experiments were conducted using a hard vascular model, which was 3D printed with transparent photosensitive resin material (Fig. 6).

Modeling of thrombus

An ideal cylindrical thrombus model was established with a diameter of 3 mm and a length of 5 mm. Two ends of the thrombus were filleted with a radius of 0.5 mm. C3D4 elements with an average size of 0.2 mm were used to mesh the thrombus.

Third-order hyperfoam material was selected for the thrombus. Its strain energy function is as follows:

$$\psi = \sum_{i=1}^{N} \frac{2\mu_i}{\alpha_i^2}[\bar{\lambda}_1^{-\alpha_i} + \bar{\lambda}_2^{-\alpha_i} + \bar{\lambda}_3^{-\alpha_i} - 3 + \frac{1}{\beta_i}(J^{-\alpha_i\beta_i} - 1)]$$

Where N is the fitting order. $\bar{\lambda}_i$ is the principal tensile ratio. μ_i, α_i and β_i are temperature-dependent material parameters (Table 3).

In vitro experiments were conducted using Thrombus Simulant (Vascular Simulations, USA), which was made of non-biological substances. According to the patient's thrombus location, the Thrombus Simulant was placed into C4 segment of the internal carotid artery.

Settings of simulation

Simulation steps are set as follows (Fig. 7):

(1) Crimping: Pull Solitaire FR 6×30 or Trevo XP ProVue 6×25 into the microcatheter respectively. Define hard contact between stent and microcatheter. And define self contact with a friction coefficient of 0.2 between surface of the stent.
(2) Positioning: Position the stent at the thrombus by moving the centerline of the microcatheter.

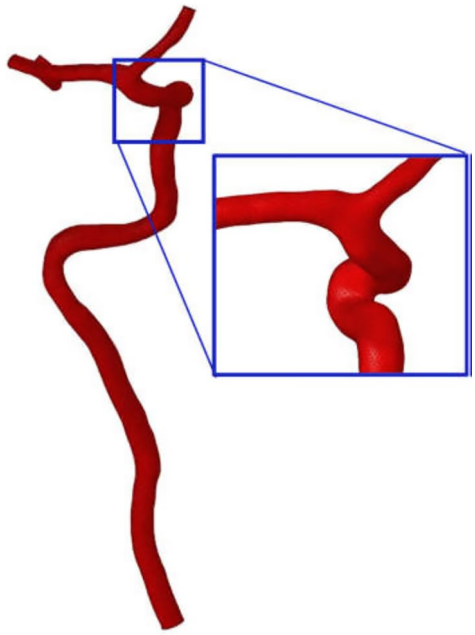

Fig. 5. Model of patient-specific blood vessels.

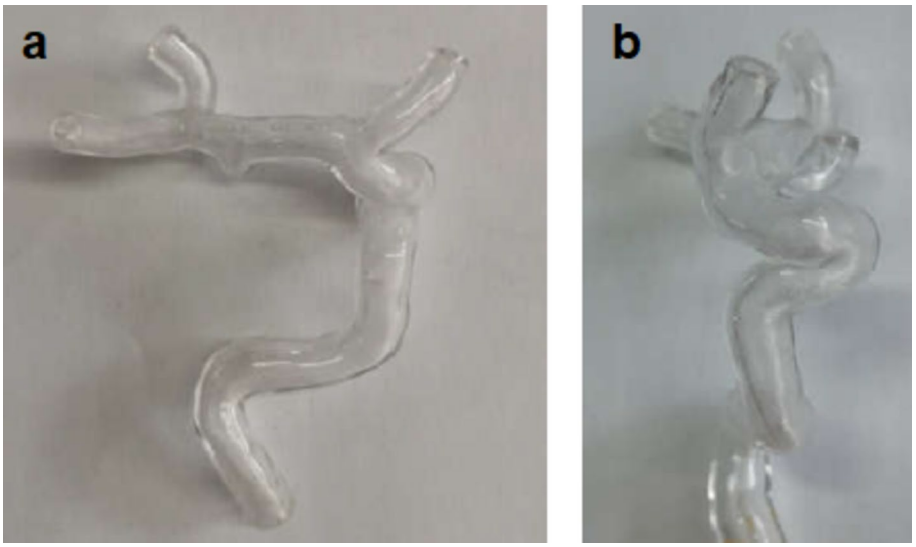

Fig. 6. 3D printed patient-specific vascular model. a, Front view; b, Side view.

μ_1/kPa	α_1	μ_2/kPa	α_2	μ_3/kPa	α_3	β_1	β_2	β_3
0.0382	5.91	0.03348	−2.9	0.02598	5.91	0.4845	0.4904	0.4845

Table 3. Material parameters of thrombus[27].

(3) Expanding: Retract the microcatheter along the centerline and release the self-expanding stent. When the stent is released, it contacts the thrombus and blood vessels. During the expanding process, the contact between stent, thrombus, and vascular wall is defined as hard contact, and the friction coefficient is set to 0.1[28]. Define frictionless self contact between surface of the thrombus.
(4) Retrieving: After the stent is completely released, apply a 25 mm displacement at the proximal end of the stent to retrieve the thrombus.

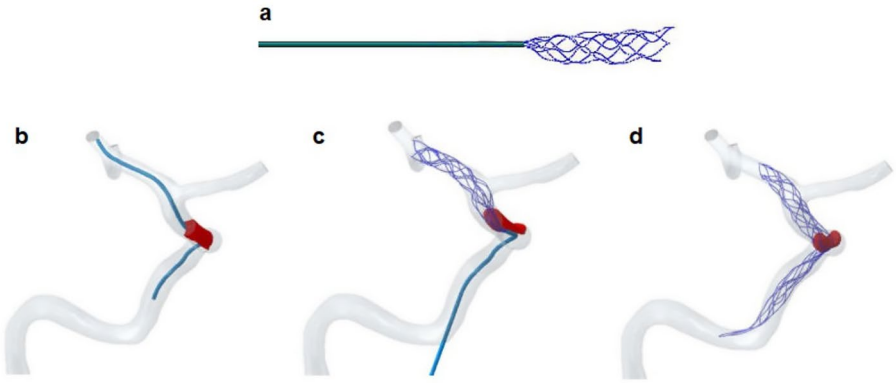

Fig. 7. Schematic diagram of thrombectomy simulation. a, Crimping; b, Positioning; c, Expanding; d, Retrieving.

Data availability

Data is provided within the manuscript.

Received: 29 October 2024; Accepted: 17 March 2025
Published online: 27 March 2025

References

1 Bose, A. et al. The penumbra system: a mechanical device for the treatment of acute stroke due to thrombosis. *Am. J. Neuroradiol.* **29**(7), 1409–1413 (2008).
2 Nogueira, R. G. et al. Thrombectomy 6 to 24 hours after stroke with a mismatch between perfusion defects and infarct. *N. Engl. J. Med.* **378**(1), 11–21 (2017).
3 Huo, X. C. & Gao, F. Chinese guidelines for endovascular treatment of acute ischemic stroke 2018. *CJS.* **13**(7), 706–729 (2018).
4 Gasou, G. et al. Tent retrievers in acute ischemic stroke: complications and failures during the perioperative period. *Am. J. Neuroradiol.* **35**(4), 734–740 (2014).
5 Liu, G. et al. Analysis of related factors for complications of mechanical thrombectomy. *J. Clin. Neurol.* **32**(4), 278–281 (2019).
6 Uchikawa, H. et al. Vasospasm as a major complication after acute mechanical thrombectomy with stent retrievers. *J. Clin. Neurosci.* **64**, 163–168 (2019).
7 Luraghi, G., Matas, J. F. R., Dubini, G., Berti, F. & Migliavacca, F. Applicability assessment of a stent-retriever thrombectomy finite-element model. *Interface Focus*. **11**(1), 20190123 (2021).
8 McCarthy, R. et al. Aspects of ischemic stroke biomechanics derived from using ex vivo and in vivo methods related to mechanical geometry. *J. Biomech.* **131**, 110900 (2022).
9 Yoo, A. J. & Andersson, T. Thrombectomy in acute ischemic stroke: challenges to procedural success. *J. Stroke*. **19**(2), 121–130 (2017).
10 Katz, J. M. et al. Understanding the radial force of stroke thrombectomy devices to minimize vessel wall injury: mechanical bench testing of the radial force generated by a novel braided thrombectomy assist device compared to laser-cut stent retrievers in simulated MCA vessel diameters. *Interv. Neurol.* **8**(2–6), 206–214 (2019).
11 Kühn, A. L., Vardar, Z., Kraitem, A., King, R. M. & Gounis, M. J. Biomechanics and hemodynamics of stent-retrievers. *J. Cerebr. Blood F. Met.* **40**(12), 2350–2365 (2020).
12 Kaneko, N., Komuro, Y., Yokota, H. & Tateshima, S. Stent retrievers with segmented design improve the efficacy of thrombectomy in tortuous vessels. *BMJ Publishing Group.* **11**, 119–122 (2019).
13 Gu, X., Qi, Y. & Erdman, A. G. The wall apposition evaluation for a mechanical embolus retrieval device. *J. Healthc. Eng.* 9592513 (2018). (2018).
14 Zhang, X., Gu, X. & Qiu, X. Biomechanical study of closed-loop thrombectomy stents. *BME.* **40**(6), 577–583 (2021).
15 Zhang, X., Gu, X., Tian, H. & Meng, F. Biomechanical study of open-loop thrombectomy stents. *J. Med. Biomech.* **36**(4), 589–595 (2021).
16 Qiu, X., Zhang, X., Gu, X., Xiao, Y. & Zhao, Y. Optimization of the mechanical properties of thrombectomy stents. *J. Med. Biomech.* **37**(3), 419–424 (2022).
17 Tutwiler, V., Singh, J., Litvinov, R. I., Bassani, J. L. & Weisel, J. W. Rupture of blood clots: mechanics and pathophysiology. *Sci. Adv.* **6**(35), eaaz496 (2020).
18 Good, B. C., Simon, S., Manning, K. & Costanzo, F. Development of a computational model for acute ischemic stroke recanalization through Cyclic aspiration. *Biomech. Model Mechanobiol.* **19**(2), 761–778 (2020).
19 Luraghi, G. et al. In vitro and in Silico modeling of endovascular stroke treatments for acute ischemic stroke. *J. Biomech.* **127**, 110693 (2021).
20 Yue, C. S. Comparative study on the effectiveness and safety of two types of thrombectomy stents in patients with acute ischemic stroke (Doctoral dissertation, Chinese People's Liberation Army Army Military Medical University) (2019).
21 Zhang, Y. J. Structural design and optimization of nickel titanium alloy intracranial thrombectomy stent (Doctoral dissertation, Huaiyin Institute of Technology) (2019).
22 Kang, D., Bu, W. & Qian, K. Progress in the application of stent-type thrombectomy devices for acute severe ischemic stroke. *CJMR*. https://doi.org/10.14033/j.cnki.cfmr.2021.04.067 (2021).
23 Mordasini, P. & Gralla, J. Developments in mechanical thrombectomy devices for the treatment of acute ischemic stroke. *Expert Rev. Med. Devices*. https://doi.org/10.1586/17434440.2015.1124019 (2016).
24 Kim, S. K., Baek, B. H., Heo, T. W. & Yoon, W. Successful cross calculation stent retriever embroidery through posterior communicating artery for acute MCA occlusion by using Trevo XP provue. *Neurointervention*. https://doi.org/10.5469/neuroint.2016.11.1.55 (2016).

25 Wei, P. Clinical efficacy of Trevo stent thrombectomy in the treatment of acute large vessel occlusive stroke (Doctoral dissertation, Guilin Medical College) (2020).
26 Finotello, A., Morganti, S. & Auricchio, F. Finite element analysis of TAVI: impact of native aortic root computational modeling strategies on simulation outcomes. *Med. Eng. Phys.* **47**, 2–12 (2017).
27 Smith, W. S. et al. Mechanical thrombectomy for acute ischemic stroke: final results of the Multi-MERCI trial. *Stroke.* **39**(4), 1205–1212 (2008).
28 Gunning, G. M. et al. Clot friction variation with fibrin content: implications for resistance to thrombectomy. *J. Neurointerv. Surg.* **10**(1), 34–38 (2018).

Author contributions
All authors have made substantial contributions to the conception and design of the study. Y.C. and Y.F. acquired the clinical data. Y.W. and K.Z. made the FEM analysis and interpretation of the data. Y.W. drafted the manuscript and S.W. revised it. All authors reviewed the final version and approved the submission.

Funding
This work was supported by the Project of National Natural Science Foundation of China[no.11872152].

Declarations

Competing interests
The authors declare no competing interests.

Ethical approval
CT angiography data was ethically approved for use by Central Hospital of Jingan District, Shanghai.

Additional information
Correspondence and requests for materials should be addressed to Y.F. or S.W.